Acta Crystallographica Section D
Biological Crystallography
ISSN 0907-4449

Cryogenic structure of the photosynthetic reaction center of *Blastochloris viridis* in the light and dark

Richard H. G. Baxter,‡ Brandon-Luke Seagle, Nina Ponomarenko and James R. Norris*

Department of Chemistry, University of Chicago, 5735 South Ellis Avenue, Chicago, IL 60637, USA

‡ Present address: Howard Hughes Medical Institute Research Laboratories, University of Texas Southwestern Medical Center, 6001 Forest Park Road, Dallas, TX 75390-9050, USA.

Correspondence e-mail: jrnorris@uchicago.edu

Received 27 August 2004
Accepted 22 February 2005

PDB References: photosynthetic reaction center, 1vrn, r1vrnsf

The structure of the *Blastochloris viridis* photosynthetic reaction center has been determined at 100 K by flash-freezing crystals. A data set to 2.2 Å resolution provides a well determined model of the wild-type protein. Of particular interest are the position, occupancy and heterogeneity of the Q_B-binding site. Data were also collected from a crystal frozen immediately after illumination. The data support predominant binding of Q_B in the proximal position in both the neutral and charge-separated states.

1. Introduction

The photosynthetic reaction center was the first integral membrane protein whose structure was determined on the molecular scale (Deisenhofer *et al.*, 1985). The function of the reaction center (RC) is to convert light energy into chemical energy *via* light-mediated electron-transfer reactions that separate charge across a biological membrane. The RCs of purple bacteria display significant structural homology to the photosystems of cyanobacteria and higher plants in the region of their primary photochemistry and continue to be relevant a model system for electron transfer, integral membrane-protein structure and quinone metabolism.

The RC of *Blastochloris viridis* consists of four polypeptide subunits. The L and M subunits have five transmembrane helices each, and form a membrane-spanning heterodimer. The H subunit has one transmembrane helix, caps the cytoplasmic side and mediates water access to the acceptor side of the electron-transfer pathway. The C subunit caps the periplasmic side and contains four tightly bound haems that form the donor side of the electron-transfer pathway. The RCs of all purple bacteria are structurally homologous to either *B. viridis* or the related species *Rhodobacter sphaeroides*, which is itself highly homologous to *B. viridis* but does not have a tightly bound cytochrome, instead being directly reduced by soluble cytochrome c_2 from the periplasm.

The *B. viridis* RC contains four cytochromes, four bacteriochlorophyll *b* molecules, two bacteriopheophytin *b* molecules, a non-haem iron, one menaquinone-9 (Q_A) and one carotenoid (1,2-dihydroneurosporene). The terminal electron acceptor within the RC is a ubiquinone-9 (UQ9) called Q_B that binds to an active site in the L subunit near the cytoplasmic side of the membrane. Q_B accepts two electrons from the primary quinone acceptor Q_A while in its active site and two protons from the cytoplasm to produce a dihydroquinol. The dihydroquinol then dissociates, followed by rebinding of neutral quinone to complete the reaction cycle.

The Q_B site is a difficult region of the RC to model owing to the relatively weak binding of the ubiquinone in its active site (K_d = 5–10 μM; Wraight *et al.*, 1984). Quantification of Q_B

with respect to Q_A suggests that only 50% of the ubiquinone is retained during normal purification (Gast *et al.*, 1985). Recent well determined models of the RC have increased the occupancy in the Q_B site by soaking or reconstituting crystals with a synthetic analog ubiquinone-2 (UQ2) that has a shorter isoprenyl tail (Lancaster & Michel, 1997; Stowell *et al.*, 1997).

Spectroscopic evidence indicates that electron transfer from Q_A to Q_B involves a 'conformational gate' (Kleinfeld *et al.*, 1984). This has been related to the two independent positions observed for Q_B within its binding pocket (Stowell *et al.*, 1997). In the original model of the *B. viridis* RC, Q_B was placed relatively deep within its binding pocket, at hydrogen-bonding distance from a ligand of the non-heme iron, HisL190 (Deisenhofer & Michel, 1989). Another position was observed in trigonal crystals of the *R. sphaeroides* RC in which the quinone was displaced 5 Å towards the protein surface (Ermler *et al.*, 1994). These positions have been labeled the 'proximal' and 'distal' positions, respectively (Lancaster & Michel, 1997).

Cryogenic data collection from *R. sphaeroides* RC crystals grown in polyethylene glycol (PEG) showed that when frozen in darkness the crystals contain Q_B predominantly in the distal position, but when frozen following illumination they contain Q_B predominantly in the proximal position (Stowell *et al.*, 1997; Axelrod *et al.*, 2000; Fritzsch *et al.*, 2002). However, a recent cryogenic structure of the *R. sphaeroides* RC from crystals grown in potassium phosphate, using phase information from an Se-MAD diffraction experiment, contains Q_B predominantly in the proximal position in the dark (Pokkuluri *et al.*, 2004).

Reanalysis of the original *B. viridis* RC data set containing UQ9 has determined that predominant distal binding for Q_B is an improved model compared with proximal binding, while UQ2-reconstituted RCs contained Q_B in the proximal position (Lancaster & Michel, 1997). In a recent time-resolved crystallographic experiment on the *B. viridis* RC, Q_B was observed in the proximal position in the dark and no large motion associated with Q_B was observed on the timescale of secondary electron transfer (Baxter, Ponomarenko *et al.*, 2004). This is in agreement with recent FTIR studies on RCs from *R. sphaeroides* that have failed to observe the changes in carbonyl vibrations expected from the different hydrogen bonding in the distal and proximal positions (Breton *et al.*, 2002, 2004; Nabedryk *et al.*, 2003; Remy & Gerwert, 2003; Breton, 2004).

To further investigate the position of Q_B within its binding site, we have obtained crystallographic data on crystals of the *B. viridis* RC frozen in the dark and following illumination. The aim of this work was to provide a more direct comparison with freeze-trapping experiments performed in *R. sphaeroides* and to obtain higher resolution information on the dark state of the *B. viridis* RC. Crystals of the *B. viridis* RC have previously been frozen to obtain the anisotropic *g*-tensor for the triplet state of the primary donor (Gast *et al.*, 1983). We further optimized these conditions and examined other possible cryoprotectants. The data obtained for the dark state extend to 2.2 Å resolution. A data set to 2.0 Å resolution has been collected at room temperature from *B. viridis* RC containing the mutation HisL168→Phe near the special pair and the herbicide terbutryn in the Q_B site (Lancaster *et al.*, 2000).

2. Methods

2.1. RC isolation and crystallization

B. viridis (ATCC 19567) cells were grown semi-anaerobically in a rich medium modified from that originally developed for *Rhodopseudomonas capsulatus* (Weaver *et al.*, 1975). RCs were purified as previously described (Lancaster & Michel, 1997; Fritzsch, 1998). The final buffer contained 20 m*M* sodium phosphate pH 6.8, 0.1% lauryldimethylamine *N*-oxide (LDAO) (Fluka) and 10 μ*M* EDTA. UV–Vis absorption spectroscopy was used to judge purity ($A_{280}/A_{830} \leq 2.1$). Crystals were grown in the dark at 291 K by sitting-drop vapour diffusion in nine-well Pyrex plates with 50 μl sample and 20 ml reservoir. The conditions for crystallization were as previously described (Baxter, Ponomarenko *et al.*, 2004). Diffraction-quality crystals belonging to the tetragonal space group $P4_32_12$ grew in 1–3 weeks in 1.8 *M* ammonium sulfate, 0.1% LDAO, 3% heptanetriol.

2.2. Cryoprotectant selection

A range of saccharides and polyalcohols were tested as additives to a standard soaking buffer. Compounds were tested in a 1 ml solution containing 0.1%(*w*/*v*) LDAO, 1%(*w*/*v*) heptanetriol, 50 m*M* sodium phosphate pH 6.0, 0.5%(*v*/*v*) triethylammonium phosphate (TEAP), 140 μ*M* UQ2 and 2.6 *M* $(NH_4)_2SO_4$. Screening was based on (i) solubility of all components, (ii) minimum concentration required for the mother liquor to glass and (iii) stability of the protein crystal in the cryoprotectant.

2.3. X-ray data collection

Crystals grown in the absence of exogenous quinone were transiently soaked in the cryobuffers described above prior to data collection. Crystals were transferred to a cryobuffer solution in an open container for 0.5–2 min and then frozen in the N_2 cryostream (100 K). Monochromatic diffraction data were collected on an ADSC Quantum-4 CCD detector at BioCARS beamline 14-BM-C, Advanced Photon Source, Argonne National Laboratory with an X-ray wavelength of 0.9 Å. Each data set was obtained over a total rotation angle of 45°. The crystal-to-detector distance was 250 mm for the dark data sets and 270 mm for the crystal flash-frozen following illumination.

2.4. Cryogenic freeze-trapping

An illumination system for cryogenic freeze-trapping was assembled in the X-ray hutch. Illumination was provided by a Xenon flash lamp (Hamamatsu L2439, 10 W maximum average power) triggered by an EG&G power supply (model PS302, 1500 V). Flash duration was 1 ms, yielding a conser-

Table 1
Data collection and refinement.

Values in parentheses are for the highest resolution shell.

Data set	Dark (glucose)	Dark (sucrose)	Light (sucrose)
Data processing			
Crystal dimensions (μm)	200 × 200 × 1000	100 × 300 × 1000	150 × 300 × 800
Unit-cell parameters (Å)	$a = b = 219.56$, $c = 112.63$	$a = b = 219.54$, $c = 112.64$	$a = b = 219.13$, $c = 112.60$
Mosaicity	0.46	0.31	0.67
Data range (Å)	50–2.20 (2.28–2.20)	50–2.40 (2.45–2.40)	50–2.60 (2.69–2.60)
No. of observations	361164	291386	223635
No. of unique reflections	121407 (8205)	98984 (6784)	76592 (6741)
Redundancy	3.0 (1.6)	2.9 (2.3)	2.9 (2.0)
No. of reflections with $I > 3\sigma(I)$	115147 (6941)	89120 (5122)	71314 (5195)
Completeness (%)	87.4 (59.9)	92.2 (64.3)	90.8 (81.0)
$\langle I\rangle/\langle\sigma\rangle$	40.6 (12.9)	32.9 (8.7)	31.5 (10.0)
$R_{\rm merge}$ (%)	2.8 (7.0)	3.2 (12.4)	3.2 (11.6)
Refinement			
Data range (Å)	20.14–2.20 (2.28–2.20)		
No. of reflections used†	119591 (7872)		
Test set (5%)	6079 (442)		
$R_{\rm cryst}$ (%)	19.1 (19.8)		
$R_{\rm free}$ (%)	21.2 (22.5)		
No. of non-H atoms	10747		
No. of solvent atoms	542		
$\langle B\rangle$ (Wilson) (Å^2)	22.6		
$\langle B\rangle$ (model) (Å^2)	29.0		
Validation			
Estimated coordinate error (Å)	0.23		
R.m.s.d. from ideal values			
Bond lengths (Å)	0.007		
Bond angles (°)	1.37		
Ramachandran analysis‡			
Most favoured (%)	891 (90.9)		
Additional allowed (%)	85 (8.7)		
Generously allowed (%)	3 (0.3)		
Disallowed (%)	1 (0.1)		
Total (%)	980 (100.0)		

† The difference in the number of reflections after scaling and those used in refinement largely arises from negative intensities rejected during conversion of intensities to structure factors. If these reflections are retained (*i.e.* set to zero) and included in refinement, $R_{\rm cryst}$ and $R_{\rm free}$ are 19.5 and 21.5%, respectively. ‡ Analysis of 1177 residues (1186 in protein less 9 in the disordered loop H46–H54): 980 non-glycine non-proline residues, ten end residues (excluding proline and glycine), 110 glycine and 77 proline residues.

vative estimate of 1–2 mJ per pulse. A fish-bowl lens focused the lamp output onto the sample with a focal length of ∼5 cm, with a spherical mirror ($f_1 = 5$ cm) serving as a back-reflector. Since the RCs were prepared without any specific oxidation or reduction, the high-potential haem in the cytochrome subunit (c_{558}, $E_{\rm m} = 380$ mV) is largely reduced (Nitschke & Rutherford, 1989). Under these conditions, the half-time of the charge-separated state is 65 s (Shopes & Wraight, 1985), giving ample time to freeze. The illumination was performed with the crystal on the goniometer immediately prior to freezing by momentarily blocking the cryostream.

2.5. Initial model building and refinement

All data sets were integrated and scaled using *HKL*2000 (Otwinowski & Minor, 1997). Intensities were converted to structure factors using the program *TRUNCATE* from the *CCP*4 program suite (Collaborative Computational Project, Number 4, 1994). The initial model was obtained by molecular replacement using the room-temperature model 1r2c (Baxter, Ponomarenko *et al.*, 2004) with Q_B and waters omitted and *B* factors reset to 30 Å^2. A test set representing 5% of the data set was used throughout refinement. Following a rotation/translation search using *EPMR* (Kissinger *et al.*, 1999), refinement was carried out using *CNS* (Brünger *et al.*, 1998). Simulated annealing of the model was used to reduce phase bias, followed by conventional positional refinement with anisotropic overall *B*-factor refinement and a bulk-solvent model, restrained individual *B*-factor refinement and further positional refinement. A second round of simulated annealing was performed omitting Q_B and the tail accessory bacteriochlorophyll $\rm Bchl_B$ in order to aid placement of the Q_B isoprenyl tail. Refinement cycles following placement of Q_B did not include simulated annealing, using $R_{\rm free}$, real-space *R* values, $2F_{\rm o} - F_{\rm c}$ or $F_{\rm o} - F_{\rm c}$ maps to judge the effects of changes to the model. Model visualization and adjustment were performed using the program *O* (Jones *et al.*, 1991).

Individual *B* factors were restrained to target deviations of 1.5 Å^2 for bonded main-chain atoms (2.0 Å^2 for side-chain atoms) and 2.0 Å^2 for main-chain atoms related by bond angles (2.5 Å^2 for side-chain atoms); however, these restraints were only weakly applied ($r_{\rm weight} = 0.05$ in *CNS*) and this combination of targets and restraints was confirmed to produce the lowest $R_{\rm free}$ compared with other values. Water molecules were initially placed in two rounds of automated placement for peaks in the $F_{\rm o} - F_{\rm c}$ map of 4σ and 3σ, respectively, which were within hydrogen-bonding distance (2.0–3.2 Å) of an O or N atom. Further manual addition or deletion of waters was made for $F_o - F_c$ peaks $>3\sigma$ by comparison with other well determined *B. viridis* RC models 1prc (Deisenhofer *et al.*, 1995), 3prc (Lancaster & Michel, 1997) and 1dxr (Lancaster *et al.*, 2000). Data-collection and refinement statistics are given in Table 1.

3. Results

3.1. Conditions for freezing

A summary of cryobuffers is given in Table 2. The monosaccharides sucrose and glucose were found to be effective cryoprotectants. Both glycerol (Fritzsch *et al.*, 2002) and ethylene glycol (Pokkuluri *et al.*, 2004) have been reported as successful cryoprotectants for *R. sphaeroides* RC trigonal crystals, but no polyalcohols were found that were suitable for freezing crystals of *B. viridis* RC. This is interesting, since the conditions of crystallization involve the same detergent (LDAO) and major amphiphile (heptanetriol), the pH differs by only 1–2 units about neutral and both involve a high ionic strength precipitant (potassium phosphate for *R. sphaeroides* RC, ammonium sulfate for *B. viridis* RC). One feature of *B. viridis* RC crystal packing is the presence of an ordered LDAO molecule that interacts with the side chain of AspH56 (Deisenhofer *et al.*, 1995). Polyalcohols may interact with detergent micelles in a manner analogous to heptanetriol and interfere with this lattice interaction. Alternatively, polyalcohols may inhibit lattice interactions involving the cytochrome subunit in *B. viridis* RC.

Table 2
Screening of cryoprotectants.

Additive‡	Solubility§ [%(*w*/*v*)]	Glass¶ [%(*w*/*v*)]	Quality	Mosaicity† 0.5 min	2 min	4 h
Sucrose	55	30	Good	N	N	N
Glucose	35	20	Good	N	N	N
Xylitol	25	—	—			
Glycerol	35	30	Variable	N	S	P
Ethylene glycol	25	15	Poor	S	P	P
PEG 200	25	25	Poor	S	P	D
1,3-Propanediol	25	20	Poor	S	P	D
1,4-Butanediol	20	—	—			

† Qualitative comparison of crystal quality for the soaking times shown. N, no noticeable effect; S, significant increase in mosaicity; P, poor crystal quality; D, crystal dissolved. ‡ The cryoprotectants PEG 400, PEG 4000 and MPD were insoluble in mother liquor at concentrations of ≥15%. § Concentrations for glucose are the highest used in these experiments, while all other concentrations are the maximum solubilities in a solution of 0.1%(*w*/*v*) 1,2,3-heptanetriol, 50 m*M* sodium phosphate pH 6.0, 0.5%(*v*/*v*) TEAP, 140 µ*M* UQ2, 2.6 *M* ammonium sulfate. ¶ The minimum concentration of cryoprotectant required for the mother liquor to glass, as determined by absence of ice rings in a static diffraction image, flash-freezing in an N_2 cryostream (100 K).

3.2. Description of the dark model

X-ray diffraction data were processed from three crystals measured at 100 K in darkness, two of which were soaked in sucrose (30%, 2.4 *M* ammonium sulfate) and one in glucose (35%, 2.6 *M* ammonium sulfate). One crystal (soaked in sucrose) was subjected to one flash from a xenon arc lamp prior to freezing, while the other two were frozen in darkness. The data sets are limited by completeness rather than $\langle I \rangle / \langle \sigma \rangle$. Refinement of the dark model was performed using the glucose data set, which had 121 407 unique reflections to 2.2 Å resolution. The final *R* factor and $R_{\rm free}$ were 19.1 and 21.2%, respectively, for a model containing 10 747 atoms including 542 water molecules.

3.2.1. Protein subunits. The overall model for the *B. viridis* RC at cryogenic temperature differs very little from that at room temperature. The r.m.s.d. between the cryogenic model and the highest resolution structure of the reaction center at room temperature, 1dxr (Lancaster *et al.*, 2000), is 0.470 Å for C_α atoms and 0.705 Å for all atoms (see supplementary material[1]). The main-chain atoms of all residues can be successfully modeled, with the exception of the final four residues of the C subunit (residues C333–C336) and a flexible loop within the H subunit (residues H45–H54). The only difference in main-chain conformation between this structure and 1dxr is a minor alteration to a small turn near the N-terminus of the H subunit (residues H7–H9). Only two residues are modeled in alternate conformations, SerL141 and MetM115, four fewer than in 1dxr. This is likely to be a consequence of the lower resolution of the structure, although it may also be indicative of the lower temperature of data collection.

3.2.2. Ordered water molecules. The cryogenic model contains 542 ordered water molecules. This number lies between those for the well determined room-temperature models 3prc (2.4 Å resolution; 87 694 reflections) and 1dxr (2.0 Å resolution; 187 940 reflections). Rather than use an empirical cutoff for the inclusion of ordered waters, a subjective assessment was made for $F_o - F_c$ peaks above the cutoff (3σ) by comparison to three other room-temperature models, 1prc, 3prc and 1dxr, the underlying assumption being that difference peaks arising from random errors are less likely to occur in the same region of space for models refined against independently collected and processed experimental data. Of the 542 waters in the model, 461 corresponded to waters found in one of the three room-temperature models used. The cryogenic model has 184 waters in common with 1prc (201 total), 337 in common with 3prc (425 total) and 436 in common with 1dxr (585 total).

3.2.3. Crystal contacts. The unit-cell parameters obtained from cryogenic data collection are not related isotropically to those of the room-temperature crystals, which have $a = b = 223.5$, $c = 113.6$ Å. While the *c* axis is 1% shorter (as also obtained for the lower resolution room-temperature data set 1r2c), the *a* and *b* axes shrink by 2%, an absolute decrease of 4 Å. Yet the refined model is not proportionally shorter than the well determined room-temperature model 1dxr. Hence, some rearrangement in the packing of protein within the crystal should be expected.

[1] Supplementary material has been deposited in the IUCr electronic archive (Reference: TM5011). Service for accessing these data are described at the back fo the journal.

B. viridis RC crystals ($P4_32_12$) contain one molecule per asymmetric unit that makes contact with five distinct neighbors by means of four distinct protein–protein interactions. Packing between the top of the cytochrome subunit (C83–C94) and a site at the interface of the C subunit with the N-terminus of the H subunit at the periplasmic membrane interface establishes the fourfold screw axis within the crystal. Comparison of symmetry-related molecules for the cryogenic model and 1dxr shows identical topology inter-protein distances within the r.m.s.d. of the two models.

Three packing interactions occur within the H subunit, each relating a set of surface residues to the same region on an adjacent molecule by a twofold rotation axis. The first comprises residues H33–H60 (excluding the disordered loop H45–H54), the second comprises residues H141–H186 and the third comprises residues H252–H256 and L20. Qualitative differences between 1dxr packing and the cryogenic model were found in each of the H-subunit interactions.

In the first packing region, ArgH33 and an ordered water (U1) form hydrogen bonds with their symmetry partners in 1dxr, but the intermediate hydrogen bonds to U1 are relatively long (3.63 and 4.13 Å). In the cryogenic model, an alternative model is proposed replacing U1 with a sulfate ion at half-occupancy, *i.e.* the ion may adopt one of two positions to form an equivalent salt bridge between the symmetry-related residues. The distances from ArgH33 $N^{\varepsilon2}$ to the closest O atom O^1 are reduced to 2.90 and 2.76 Å and electroneutrality is maintained.

In the second region, the hydroxyl O atom of ThrH141 forms a hydrogen-bonding interaction with the carbonyl O atom of its symmetry partner in 1dxr, while the $C^{\beta}-C^{\beta}$ distance is 5.21 Å. In the cryogenic model the $C^{\beta}-C^{\beta}$ distance is reduced to 3.64 Å, but the side chain adopts a different rotamer that does not form a hydrogen bond to the main chain. In the center of the region an ordered water molecule was found at a special position (W1541) that introduces an ordered chain of three waters between ArgH153 and its symmetry partner.

In the third packing region, GluH255 $O^{\varepsilon2}$ forms an interaction with its symmetry partner through two ordered waters and their symmetry partners in 1dxr, comprising five hydrogen bonds and an $O^{\varepsilon2}-O^{\varepsilon2}$ distance of 6.45 Å. In the cryogenic model the $O^{\varepsilon2}-O^{\varepsilon2}$ distance is reduced to 4.02 Å and one of the waters occupies a special position approximately 3 Å from the origin of the unit cell. In this same region GluH252 adopts a different side-chain conformation, resulting in an additional water-mediated interaction with the hydroxyl O atom of SerH256.

3.2.4. Cofactors. All cofactors are included in the refined model at full occupancy, with the exception of BPh_B, for which the occupancies of the final nine atoms of the phytyl tail were set to an occupancy of zero, and the ubiquinone, which is modelled with an aliphatic tail of only seven isoprenyl units. In addition, six LDAO detergent molecules and seven sulfate ions are included in the model (the headgroup of the fifth detergent is at zero occupancy).

Particular attention was paid to the Q_B-binding site in the course of refinement. A simulated-annealing omit map revealed clear density for Q_B in the proximal binding site (Fig. 1). The optimal orientation for the isoprenyl tail follows that of the ubiquinone model $1prc_{new}$ (Lancaster & Michel, 1997). An alternate orientation was tested that diverges following the first isoprenyl unit, which is similar to the orientation of the LDAO molecule that occupies the Q_B site in Q_B-depleted reaction centers (Lancaster & Michel, 1997). This orientation was discarded as it led to a higher real-space *R* factor and a higher overall *R* factor for the model.

Despite the obviously predominant location of Q_B in the proximal position, the experimental density suggests that the Q_B site is heterogeneously occupied. The density appears to be too large for the substituted aromatic ring at its point of connection to the isoprenyl tail (Fig. 1*a*). The average atomic *B* factor for the Q_B headgroup (substituted ring and first isoprenyl unit, *i.e.* UQ1) is 49.3 $Å^2$, almost twice that of the surrounding side chains (L189, L190, L212, L213, L216, L222–L224) of 28.78 $Å^2$ or the model in general. This is true regardless of whether the entire isoprenyl tail is included in the refinement. The use of a 'relative quinone quality' factor (RQQ) has been suggested as a method of estimating the quality of Q_B-site models (Lancaster, 1999). This is the ratio of the average cofactor quality $CQ = 100Q\exp(-B/4d_{\min}^2)$, where Q is the occupancy, B the atomic temperature factor and $d_{\min}$ the maximum resolution of the data set (Arnold & Rossmann, 1990), for the headgroup of the quinone *versus* that for the porphyrin rings of the special pair. For the cryogenic model, the RQQ values of Q_A and Q_B at full occupancy are 0.95 and 0.16, respectively.

The most likely cause of the poor-quality Q_B model is that the Q_B site is not fully occupied. By chemical analysis, it is known that up to 50% of endogenous Q_B is lost during RC protein purification using standard procedures (Gast *et al.*, 1985). The previous room-temperature model 1r2c from this laboratory reported the quinone occupancy to be 0.6 ± 0.1 based on restrained atomic *B*-factor refinement of a UQ2 Q_B model at differing occupancies (Baxter, Ponomarenko *et al.*, 2004). Hence, we chose to scale the atomic *B* factors of our full-occupancy Q_B model to those of the surrounding amino-acid side chains and then refined the occupancy of the ubiquinone molecule. The occupancy of the resulting model was 0.56, leading to an RQQ_B of 0.29. It should be noted that the average *B* factor for atoms of the special pair are below average for the entire structure (the quality factor for the Q_B pocket itself is 0.52). Since the refined occupancy represents a reasonable expectation for the sample, this value was used in the model 1vrn deposited in the PDB.

3.3. Freeze-trapping

It has been hypothesized (Stowell *et al.*, 1997) that Q_B, which is bound in the distal position in the neutral state, will be found in the proximal position following its photoreduction of the reaction center. If this is the case, then in principle an occupancy shift could be detected in a difference Fourier map of a crystal frozen under illumination compared with one frozen in the dark. Fig. 2 shows unweighted F_o maps for the Q_B site obtained from the dark (Fig. 2*a*) and light (Fig. 2*b*) sucrose data sets. A difference Fourier map ($F_{light} - F_{dark}$; Fig. 2*c*) was calculated by first scaling the light data sets to the dark data set using the program *SCALEIT* from the *CCP*4 program suite (Collaborative Computational Project, Number 4, 1994) and then taking the difference of those structure factors in common. The resulting differences were weighted according to their relative error (Ursby & Bourgeois, 1997). The set of phases used to calculate all three maps were obtained from the simulated-annealing model omitting Q_B and the accessory $BChl_B$ tail (see Fig. 1*a*). No significant features in this map can be correlated with an occupancy shift of quinone between the distal and proximal positions. Some significant features are observed on GluL212 and several other residues in the protein, including the two most distal cytochromes, which are interpreted as arising from radiation damage (Baxter, Seagle *et al.*, 2004).

4. Discussion

The structure of the *B. viridis* RC at cryogenic resolution provides additional information regarding the position and relative heterogeneity of the secondary quinone acceptor in its binding site. Although technically the most well determined structure of the wild-type *B. viridis* RC to date, it differs very little from the most well determined structure of all *B. viridis* RCs, 1dxr (which contains a single amino-acid substitution HisL168→Phe and terbutryn bound in the Q_B pocket). The effective resolution of the model is somewhat limited owing to lack of completeness in the higher resolution shells, but the electron-density maps are of good quality. The slight shrinkage of the unit-cell parameters arises from some rearrangement of crystal packing involving regions of the H subunit.

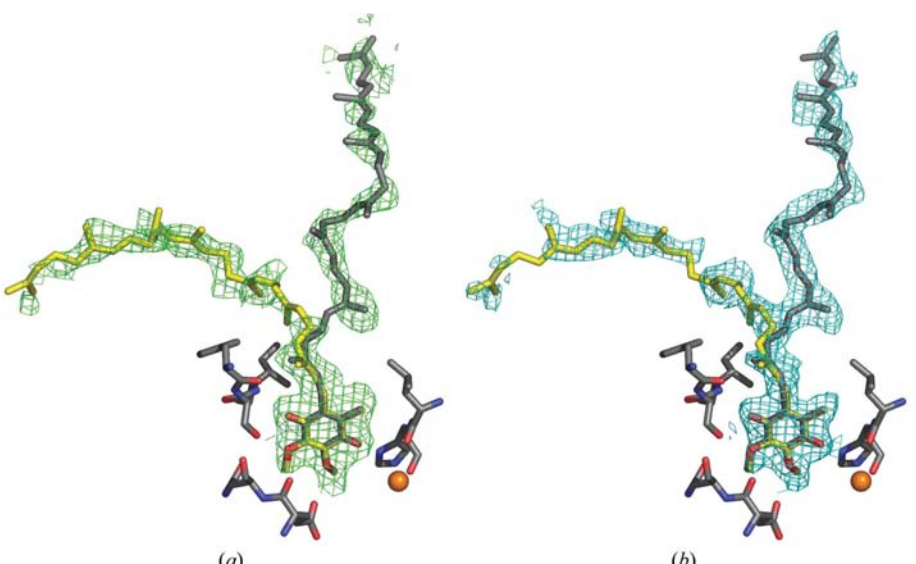

Figure 1
Simulated-annealing $F_o - F_c$ (*a*) and refined $2F_o - F_c$ (*b*) electron density for Q_B in its active site. Maps contoured at 1.5σ and 1.0σ, respectively. The alternate model for the quinone is shown in yellow. Figs. 1 and 2 were produced using *PyMOL* (DeLano, 2002).

4.1. Modelling the Q_B site

We have paid most attention to the Q_B pocket during refinement for three reasons. Firstly, the majority of recently reported structures have placed Q_B in the distal position, as has reanalysis of the original *B. viridis* RC data set. Yet the structure of the RC–UQ2 complex (Lancaster & Michel, 1997) reports only proximal binding of ubiquinone. We sought to resolve this discrepancy by obtaining further experimental data on

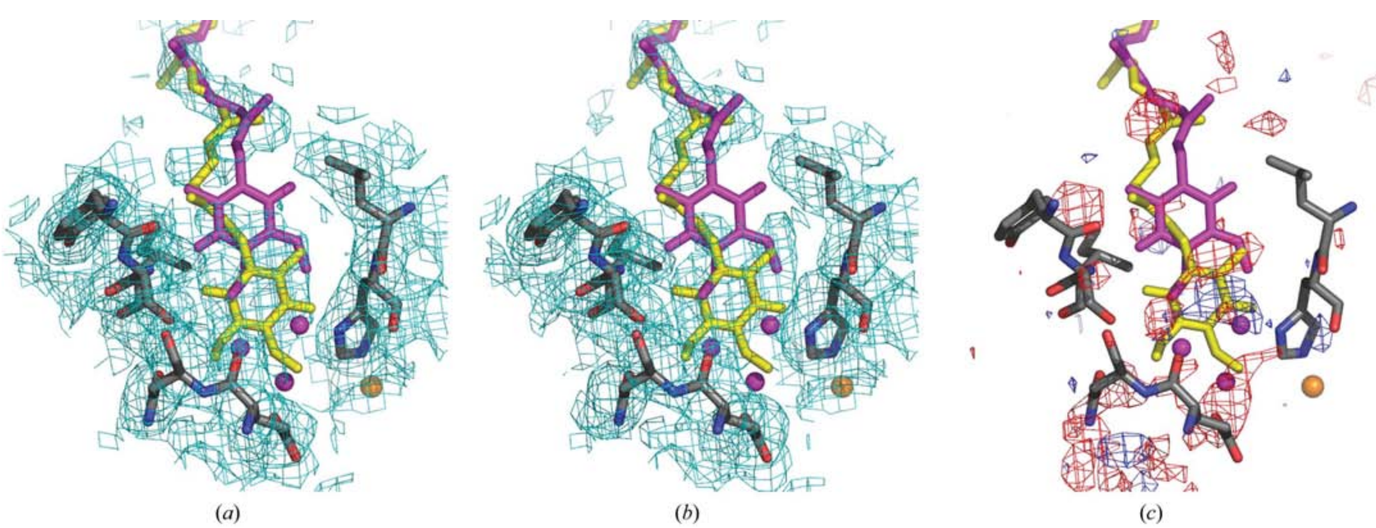

Figure 2
Unweighted F_o map of the Q_B site for (*a*) dark sucrose and (*b*) light sucrose data sets and (*c*) weighted difference Fourier map $F_{light} - F_{dark}$. Contours are at 0.5σ for F_o maps and +3σ (blue) and −3σ (red) for difference map. The distal (magenta) and proximal (yellow) models are shown for comparison.

the wild-type structure. Also, given recent negative results from time-resolved experiments regarding movement of quinone from the distal to the proximal binding site (Remy & Gerwert, 2003; Baxter, Ponomarenko *et al.*, 2004), we wished to determine if the relatively low resolution of the room-temperature model 1r2c was related to the inability to observe distal binding of Q_B or if freezing had a significant influence on the quinone position in the *B. viridis* RC. Finally, the development of cryogenic conditions has allowed us to attempt to directly repeat the freeze-trapping experiments that have been performed multiple times in *R. sphaeroides* (Stowell *et al.*, 1997; Axelrod *et al.*, 2000; Fritzsch *et al.*, 2002). Our results confirm the room-temperature model 1r2c in that Q_B is bound predominantly in the proximal position, as is intuitively clear from the SA omit map (Fig. 1). The refined occupancy of 0.56 for the proximal model agrees closely with the earlier estimate for Q_B and is similar to that expected from a standard purification protocol. Hence, the conditions of freezing do not appear to have any effect on the quinone position.

Some additional ambiguous density in the Q_B site is most likely to represent a heterogeneous distribution of different structures within the crystal. Three possible models exist for the Q_B site: Q_B in the proximal position (*e.g.* 2prc for *B. viridis* RC, 1aig and 1qov for *R. sphaeroides* RC), Q_B in the distal position (*e.g.* $1prc_{new}$ for *B. viridis* RC, 1pcr and 1aij for *R. sphaeroides* RC) and an empty site occupied by several ordered water molecules and a detergent molecule (3prc for *B. viridis* RC). Density within the Q_B site for the RC in the dark state has been interpreted by previous authors as follows: in *R. sphaeroides*, a majority distal population and minor proximal/empty population (Stowell *et al.*, 1997), 55% distal and 45% proximal (Fritzsch *et al.*, 2002), 16% distal, 64% proximal and 20% empty (Pokkuluri *et al.*, 2004); in *B. viridis*, 30% distal, 20% proximal and 50% empty (Lancaster, 1999). In the case of this structure, the occupancy of the proximal position is 60%, with the remaining density attributable to the distal position or empty sites. While the assignment of absolute percentages is not physically meaningful at this resolution, we estimate the distal occupancy cannot be more than 15%. In other words, the observed density in our structure is most comparable to that of Pokkuluri *et al.* (2004) as opposed to other reported structures. It is qualitatively different from that of the reanalyzed *B. viridis* RC data set (Lancaster & Michel, 1997), for which the distal model was the predominant conformation.

4.2. Freeze-trapping

We have previously concluded on the basis of a time-resolved crystallographic experiment that movement of quinone from the distal to the proximal position could not be the 'conformational gate' that is believed to operate during secondary electron transfer within the reaction center (Baxter, Ponomarenko *et al.*, 2004). In doing so, we provided a simulation as evidence that even a 10% occupancy shift in quinone position should be resolvable by low-resolution data with experimental noise features. In this case, if we assume that 10% of Q_B is in the distal position and gives rise to the difference features observed in Fig. 2, then a saturating illumination of the crystal prior to freezing would generate an observable feature in the difference Fourier map if this subpopulation did indeed undergo a change in position owing to electron transfer.

However, the assumption of saturating illumination is probably not valid. Measurement of photoactivation in other time-resolved crystallographic experiments, as well as recent spectroscopic studies of *B. viridis* RC crystals (Baxter, 2004), suggests that 50% illumination is achievable with a laser illumination system. The original crystallographic freeze-trapping experiment conducted using the *R. sphaeroides* RC (Stowell *et al.*, 1997) provided evidence of saturating illumination from an incandescent source, but the requisite measurements were not conducted on the illumination system used in this experiment. A 5% occupancy shift would be realistic from this experiment, which cannot be definitely said to be observable.

However, the issue of light-induced conformational changes within the Q_B pocket is moot if Q_B does not bind predominantly in the distal position in the dark, as is deduced from this structure. One advantage of the cryogenic data collection in regard to the dark model of Q_B is the issue of X-ray-induced reduction. One may postulate that direct reduction by X-ray radiation may generate the semiquinone species during the course of data collection at room temperature or that a slow rate of charge recombination in a time-resolved pump-probe experiment generates a photo-stationary charge-separated state. Both these effects are negated if the crystal is frozen prior to X-ray exposure as in this case.

4.3. Influence on quinone position

The question remains as to why multiple crystallographic models of bacterial reaction centers possess Q_B bound in the distal position while others do not and why evidence of the distal position for Q_B is not found in FTIR studies. Since the first observation of the distal binding site, the different preference for Q_B binding has been attributed to the presence of ubiquinol (Ermler *et al.*, 1994), ubiquinone isoprenyl chain length (Lancaster & Michel, 1997), electronic state (Q_B *versus* Q_B^-; Stowell *et al.*, 1997), protonation of certain amino acids in the Q_B pocket (Grafton & Wheeler, 1999) and the temperature of data collection and different cryoprotectants (Pokkuluri *et al.*, 2004). Furthermore, site-directed mutations affecting the Q_A or Q_B pocket influence the crystallographically observed position of Q_B (McAuley *et al.*, 2000; Kuglstatter *et al.*, 2001; Pokkuluri *et al.*, 2002; Xu *et al.*, 2004), variously attributed to the mutation's influence on one of the factors above. To this we can only add the pH of the mother liquor, which varies from 6.0 in *B. viridis* RC (2prc and this study) to pH 8.5 in *R. sphaeroides* RC (*e.g.* 1rzh). Frankly, we are unable to determine any single factor that can explain the distribution of positions adopted by Q_B in these different structures.

Without careful comparison of conditions for sample preparation and additional measurements to test the occupancy and electronic state of Q_B within the crystal, heterogeneous and varying occupancy within the Q_B site will continue to be a feature of bacterial RC structures. Without experimental verification by other means, however, we question the necessity of incorporating the distal position for Q_B at the beginning of an overall reaction mechanism for secondary electron transfer. We agree with the statement that

> the distally bound Q_B observed in the crystal structures 1prc$_{new}$, 1pcr and 1aij can be interpreted as unproductively bound quinone which must first undergo ring flipping ... before it can be reduced at the proximal site

(Zachariae & Lancaster, 2001). We see no reason, however, why ubiquinone cannot be envisaged to enter the proximal position directly from the membrane phase *in vivo*.

The authors would like to thank Phoebe Rice and Xiaojing Yang for assistance with in-house screening. This work was supported by DOE FG02-96ER14675 to JRN; RB was supported by Burroughs Wellcome Fund Interfaces in Science Program 1001774, coordinated by Drs Steven Kron and Norbert Scherer. BS was supported by a summer research scholarship from the Richter Fund, University of Chicago. Use of the Advanced Photon Source was supported by the US Department of Energy, Basic Energy Sciences, Office of Science, under Contract No. W-31-109-Eng-38. Use of BioCARS Sector 14 was supported by the National Institutes of Health, National Center for Research Resources, under grant number RR07707.

References

Arnold, E. & Rossmann, M. G. (1990). *J. Mol. Biol.* **211**, 763–801.
Axelrod, H. L., Abresch, E. C., Paddock, M. L., Okamura, M. Y. & Feher, G. (2000). *Proc. Natl Acad. Sci. USA*, **97**, 1542–1547.
Baxter, R. H. G. (2004). PhD thesis, University of Chicago, USA.
Baxter, R. H. G., Ponomarenko, N., Šrajer, V., Pahl, R., Moffat, K. & Norris, J. R. (2004). *Proc. Natl Acad. Sci. USA*, **101**, 5982–5987.
Baxter, R. H. G., Seagle, B.-L., Ponomarenko, N. & Norris, J. R. (2004). *J. Am. Chem. Soc.* **126**, 16728–16729.
Breton, J. (2004). *Biochemistry*, **43**, 3318–3326.
Breton, J., Boullais, C., Mioskowski, C., Sebban, P., Baciou, L. & Nabedryk, E. (2002). *Biochemistry*, **41**, 12921–12927.
Breton, J., Wakeham, M. C., Fyfe, P. K., Jones, M. R. & Nabedryk, E. (2004). *Biochim. Biophys. Acta*, **1656**, 127–138.
Brünger, A. T., Adams, P. D., Clore, G. M., DeLano, W. L., Gros, P., Grosse-Kunstleve, R. W., Jiang, J.-S., Kuszewski, J., Nilges, M., Pannu, N. S., Read, R. J., Rice, L. M., Simonson, T. & Warren, G. L. (1998). *Acta Cryst.* D**54**, 905–921.
Collaborative Computational Project, Number 4 (1994). *Acta Cryst.* D**50**, 760–763.
Deisenhofer, J., Epp, O., Miki, K., Huber, R. & Michel, H. (1985). *Nature (London)*, **318**, 618–624.
Deisenhofer, J., Epp, O., Sinning, I. & Michel, H. (1995). *J. Mol. Biol.* **246**, 429–457.
Deisenhofer, J. & Michel, H. (1989). *EMBO J.* **8**, 2149–2170.
DeLano, W. L. (2002). *The PyMOL Molecular Graphics System*, http://www.pymol.org.
Ermler, U., Fritzsch, G., Buchanan, S. K. & Michel, H. (1994). *Structure*, **2**, 925–936.
Fritzsch, G. (1998). *Methods Enzymol.* **297**, 57–77.
Fritzsch, G., Koepke, J., Diem, R., Kuglstatter, A. & Baciou, L. (2002). *Acta Cryst.* D**58**, 1660–1663.
Gast, P., Michalski, T. J., Hunt, J. E. & Norris, J. R. (1985). *FEBS Lett.* **179**, 325–328.
Gast, P., Wasielewski, M. R., Schiffer, M. & Norris, J. R. (1983). *Nature (London)*, **305**, 451–452.
Grafton, A. K. & Wheeler, R. A. (1999). *J. Phys. Chem. B*, **103**, 5380–5387.
Jones, T. A., Zou, J. Y., Cowan, S. W. & Kjeldgaard, M. (1991). *Acta Cryst.* A**47**, 110–119.
Kissinger, C. R., Gehlhaar, D. K. & Fogel, D. B. (1999). *Acta Cryst.* D**55**, 484–491.
Kleinfeld, D., Okamura, M. Y. & Feher, G. (1984). *Biochemistry*, **23**, 5780–5786.
Kuglstatter, A., Ermler, U., Michel, H., Baciou, L. & Fritzsch, G. (2001). *Biochemistry*, **40**, 4253–4260.
Lancaster, C. R. D. (1999). *Biochem. Soc. Trans.* **27**, 591–596.
Lancaster, C. R. D., Bibikova, M. V., Sabatino, P., Oesterhelt, D. & Michel, H. (2000). *J. Biol. Chem.* **275**, 39364–39368.
Lancaster, C. R. D. & Michel, H. (1997). *Structure*, **5**, 1339–1359.
McAuley, K. E., Fyfe, P. K., Ridge, J. P., Cogdell, R. J., Isaacs, N. W. & Jones, M. R. (2000). *Biochemistry*, **39**, 15032–15043.
Nabedryk, E., Breton, J., Sebban, P. & Baciou, L. (2003). *Biochemistry*, **42**, 5819–5827.
Nitschke, W. & Rutherford, A. W. (1989). *Biochemistry*, **28**, 3161–3168.
Otwinowski, Z. & Minor, W. (1997). *Methods Enzymol.* **276**, 307–326.
Pokkuluri, P. R., Laible, P. D., Crawford, A. E., Mayfield, J. F., Yousef, M. A., Ginell, S. L., Hanson, D. K. & Schiffer, M. (2004). *FEBS Lett.* **570**, 171–174.
Pokkuluri, P. R., Laible, P. D., Deng, Y. L., Wong, T. N., Hanson, D. K. & Schiffer, M. (2002). *Biochemistry*, **41**, 5998–6007.
Remy, A. & Gerwert, K. (2003). *Nature Struct. Biol.* **10**, 637–644.
Shopes, R. J. & Wraight, C. A. (1985). *Biochim. Biophys. Acta*, **806**, 348–356.
Stowell, M. H. B., McPhillips, T. M., Rees, D. C., Soltis, S. M., Abresch, E. & Feher, G. (1997). *Science*, **276**, 812–816.
Ursby, T. & Bourgeois, D. (1997). *Acta Cryst.* A**53**, 564–575.
Weaver, P. F., Wall, J. D. & Gest, H. (1975). *Arch. Microbiol.* **105**, 207–216.
Wraight, C. A., Stein, R. R., Shopes, R. J. & McComb, J. C. (1984). *Advances in Photosynthesis Research*, Vol. 1, edited by C. Sybesma, pp. 629–636. Dordrecht: Nijhoff/Junk.
Xu, Q., Axelrod, H. L., Abresch, E. C., Paddock, M. L., Okamura, M. Y. & Feher, G. (2004). *Structure*, **12**, 703–715.
Zachariae, U. & Lancaster, C. R. D. (2001). *Biochim. Biophys. Acta*, **1505**, 280–290.